Article

JOURNAL OF COMPOSITE MATERIALS

Journal of Composite Materials
0(0) 1–16

DOI: 10.1177/0021998316669875
jcm.sagepub.com
SAGE

Nonconformal mesh-based finite element strategy for 3D textile composites

B Wucher[1], S Hallström[2], D Dumas[1], T Pardoen[3], C Bailly[4], Ph Martiny[5] and F Lani[6]

Abstract

A finite element procedure is developed for the computation of the thermoelastic properties of textile composites with complex and compact two- and three-dimensional woven reinforcement architectures. The purpose of the method is to provide estimates of the properties of the composite with minimum geometrical modeling effort. The software TexGen is used to model simplified representations of complex textiles. This results in severe yarn penetrations, which prevent conventional meshing. A non-conformal meshing strategy is adopted, where the mesh is refined at material interfaces. Penetrations are mitigated by using an original local correction of the material properties of the yarns to account for the true fiber content. The method is compared to more sophisticated textile modeling approaches and successfully assessed towards experimental data selected from the literature.

Keywords

Mechanical properties, finite element analysis, three-dimensional reinforcement

Introduction

The increasing use of textile composites in structural components requires increasingly reliable and efficient design tools to guide the manufacturing operations and predict the structural behavior. Given the complexity of modern reinforcement topology, these tools generally consider the impregnated textiles as homogeneous materials at the structural scale. Thus, other predictive methods are in turn needed to determine the homogeneous behavior of the composites based on the microstructure and on the properties of the constituents. The vast fields of numerical homogenization and textile modeling serve this purpose. The wide variety of textile configurations requires these tools to be universal and as user-friendly as possible. While the condition of universality is met by a number of techniques, their use often necessitates considerable development and expertise, thus limiting their applicability in the industrial world.

Homogenization of fiber-reinforced polymers, and more specifically of textile composites, has received major attention in the last decades. It consists in modeling a representative volume element (RVE) of the textile architecture and, using a homogenization scheme, to determine the thermomechanical behavior of the RVE. Textile modeling and homogenization schemes constitute two separate lines of research, of which a brief and nonexhaustive review is presented here.

Pioneering works in homogenization of woven composites include that of Ishikawa and Chou,[1] namely the mosaic, bridging and fiber undulation models to predict the in-plane properties of woven textiles. These models are based on classical laminate theory and are thus based on the simple iso-strain assumptions. Other analytical or semi-analytical schemes rely on the complementary variational principle, like the approach proposed by Vandeurzen et al.[2,3] or the generalized

[1]Methods for Structural Applications and Processes, Cenaero, Belgium
[2]Department of Aeronautical and Vehicle Engineering, KTH Royal Institute of Technology, Sweden
[3]Institute of Mechanics, Materials and Civil Engineering, Université catholique de Louvain, Belgium
[4]Institute of Condensed Matter and Nanosciences, Université catholique de Louvain, Belgium
[5]e-Xstream Engineering, MSC Software, Belgium
[6]Any-Shape, Belgium

Corresponding author:
B Wucher, Methods for Structural Applications and Processes, Cenaero, Rue des Frères Wright 29, B-6041 Gosselies, Belgium.
Email: benoit.wucher@cenaero.be

method of cells.[4] The latter is quite universal and has been exploited for failure modeling of three-dimensional (3D) woven textiles by Prodromou et al.[5] Mean-field techniques such as the Mori–Tanaka method are very efficient for predicting homogenized properties.[6] However, most analytical solutions, even with rich kinematics and high-order representation of the geometry, generally lead to rather poor predictions of the magnitude of the local or per-phase average fields.[7]

The advent of high-performance computing has made possible the use of finite element (FE)-based approaches even for complex architectures, which can provide reference solutions as a basis for the assessment of the aforementioned analytical methods. FE techniques can be further divided into two categories:

- Classical approaches use either conformal meshes of yarns and of the resin-rich domains, or nonconformal meshes that do not align element edges with yarn boundaries, of which a typical example is voxel meshing. Although conformal meshes provide better means for modeling detailed microscopic stress states inside the RVE, modeling and meshing properly the geometry of the thin resin layers appearing where the yarns come into contact can be difficult. Among other techniques, an artificial resin layer between the yarns can be added.[8,9] Voxel approaches[10–17] describe the textile as a grid of uniformly-sized hexahedra. In essence, the irregularity of the modeled yarn boundaries then leads to spurious stress concentrations but the approach is nevertheless widely used in linear elastic homogenization and in the context of failure analysis,[12,17] especially when generating conformal meshes becomes complicated.
- Other approaches consist in modifying the FE formulation to take into account the presence of the yarns inside the matrix. Independent mesh methods,[18] mesh superposition,[19] or the binary model of Cox et al.[20] are examples of such approaches.

Textile modeling is the step preceding homogenization and is of equal importance. To this day, the WiseTex software package[8,21–23] and the Digimat tool suite[24,25] probably offer the most complete homogenization solutions. WiseTex provides a framework to represent a wide range of textiles with analytical[23] or FE tools[8] for permeability[22] or mechanical analysis. Digimat offers a range of capabilities to model not only textile composites but also short-fiber-reinforced plastics and discontinuous fiber composites both with FE-based and semi-analytical methods. The TexGen software package[26] provides an efficient open-source alternative, but its capabilities are not as broad. Very fine textile modeling can be achieved for instance through X-ray computed tomography (micro-CT),[11] textile compacting FE analysis,[27,28] yarn inflation FE analysis,[29] level-set-based approaches,[30] or yarn discretization procedures.[31] Most of these techniques rely on heavy calculations, and are sometimes degraded by the obligation to use a voxel mesh.[11,12] In any case, modeling one RVE of the composite very finely (as with micro-CT) is not necessarily more relevant than modeling a simplified idealized RVE based on averaged measurements over the entire composite.[13]

One of the main purposes of refined textile modeling is to avoid material overlap, also referred to as penetrations. One strategy is to start from a simplified geometrical model of the yarns, and to remove regions with penetrations a posteriori, either by geometrical considerations[21,32,33] or by FE analysis.[8] These solutions are, however, usually not very generic or are limited to small penetrations.

The present work investigates an alternative approach, where the main idea is not to avoid or suppress penetrations, but to ally simple geometrical modeling with the power and universality of classical FE analysis. To this end, textiles are modeled using the open-source software TexGen by keeping a few key parameters comparable to the real textile, such as fiber content, crimp, or yarn paths. These geometrical simplifications lead to penetrations for highly compacted textiles,[13] i.e. when the yarns occupy a large portion of the volume of the RVE, since increasing the yarn volume necessarily makes the yarns closer to one another. These penetrations constitute inextricable obstacles to conventional meshing and, therefore, a nonconformal mesh is used. With the intent of rationalizing the mesh size compared to classical hexahedral voxels, the mesh is unstructured and is refined at the yarn–matrix interface. Penetrations are compensated for by locally adapting the fiber volume fraction inside the yarns. The proposed methodology can be applied to any textile but is more relevant for the ones that are complex to represent geometrically, namely 3D woven textiles. Although the framework is not limited to linear elasticity, its extension to other considerations such as failure mechanisms will necessitate adjustments and particular care. It is therefore left out of the scope of this paper, focusing on the method and its assessment more than on its applications. The outline of the paper is the following. The upcoming section starts with the development of a nonconformal meshing procedure, enabling the FE representation of penetrated textiles. Next section details the methodology to compensate textile penetrations and assesses its accuracy on a simplified test case. Finally, the last section presents results obtained within the present framework for 3D textiles, examples from the literature.

Nonconformal meshing

The starting point of the present methodology is to perform homogenization FE analysis on the textile models containing material penetrations. Penetrations mostly arise when the textile exhibits a high yarn volume fraction or when the modeling approach is not refined enough. Figure 1 illustrates typical penetrations, which can occur when dealing with a plain-weave fabric.

When the volume fraction of the yarns within the RVE is increased, penetrations emerge and suppressing them with maintained yarn volume fraction would require relocation of material from regions where yarns overlap to regions where there is still available open space. Such adjustments are most commonly performed via iterative geometrical considerations or FE simulations,[8,21,32,33] and they become increasingly more complex as the model reaches a high level of compaction. If penetrations are not mitigated, which is the case in the present work, meshing the RVE of Figure 1 with a conventional method would require the software to automatically detect the penetration volume and to mesh it separately from the remaining yarn volumes. In a general case of e.g. a 3D textile model, the overlapping regions can be of complex shape, which make cleaning operations complicated. Nonconformal meshing might then be a better alternative. The most classical approach would be to use a uniformly sized voxel mesh. However, it has the disadvantages of being both over-refined in the resin region and not refined enough around the yarn boundaries, leading to irregular interfaces and spurious stress concentrations. A technique to produce a voxel mesh refined at the yarn boundaries, similar to the quadtree procedure, was developed by Kim and Swan.[16] It has the additional constraint that it provides a disconnected mesh. Therefore, cumbersome post-treatment is needed in order to create suitable multipoint constraints (MPCs). Here, another approach is adopted to rationalize the mesh size while keeping a classical connected mesh, illustrated for a penetrating plain-weave in Figure 2. The penetrations are exaggerated for the sake of clarity.

An improved nonconformal representation of the yarn boundaries is ensured through a mesh adaptation procedure. To this end, a signed distance field d, or level-set, is computed as proposed by Sonon and Massart[30]

$$d(x, y, z) = \max_i \left\{ \min \left[d_i, d_i - \left(\max_{j \neq i} d_j \right) \right] \right\} \quad (1)$$

where d_i is the signed distance between the point $P(x, y, z)$ and the yarn recorded with number i. d_i is positive if P is inside the yarn and negative if it is outside. This convention is opposite to that of Sonon and Massart[30] in order to be consistent with past developments by the authors. As can be seen in Figure 2(b), the iso-zero of the level-set d (i.e. where d is equal to zero) captures, in a very generic manner, the yarn boundaries as well as the iso-distance between two yarn boundaries in the penetrating regions. In a subsequent step, the open-source meshing software GMSH[34] is used for the mesh adaptation procedure based on the level-set as an input to dictate the element size

$$s(x, y, z) = \max(m, \ \min(M, \ \beta |d(x, y, z)|)) \quad (2)$$

where s is the mesh size field, d is the signed distance field, m and M are the user-defined minimum and maximum mesh sizes, respectively, and β is the imposed

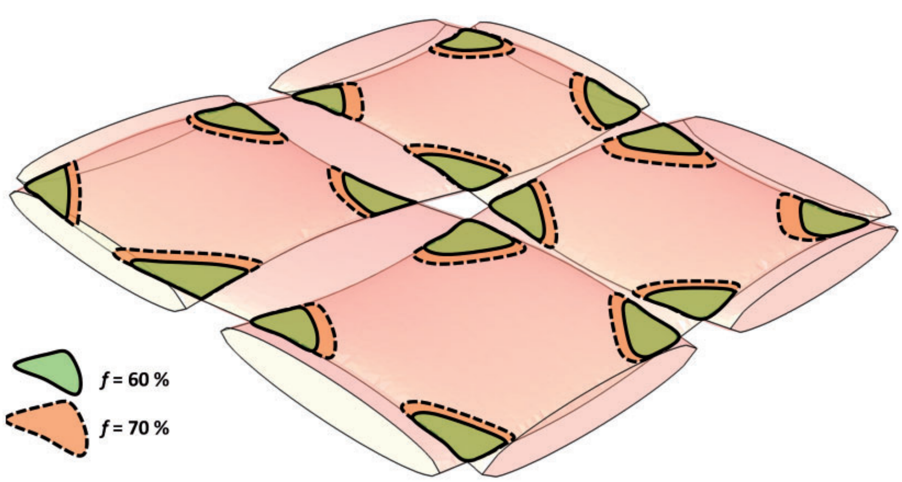

Figure 1. Plain-weave textile with an illustration of typical penetration locations when the volume fraction of the yarns within the RVE f is high.

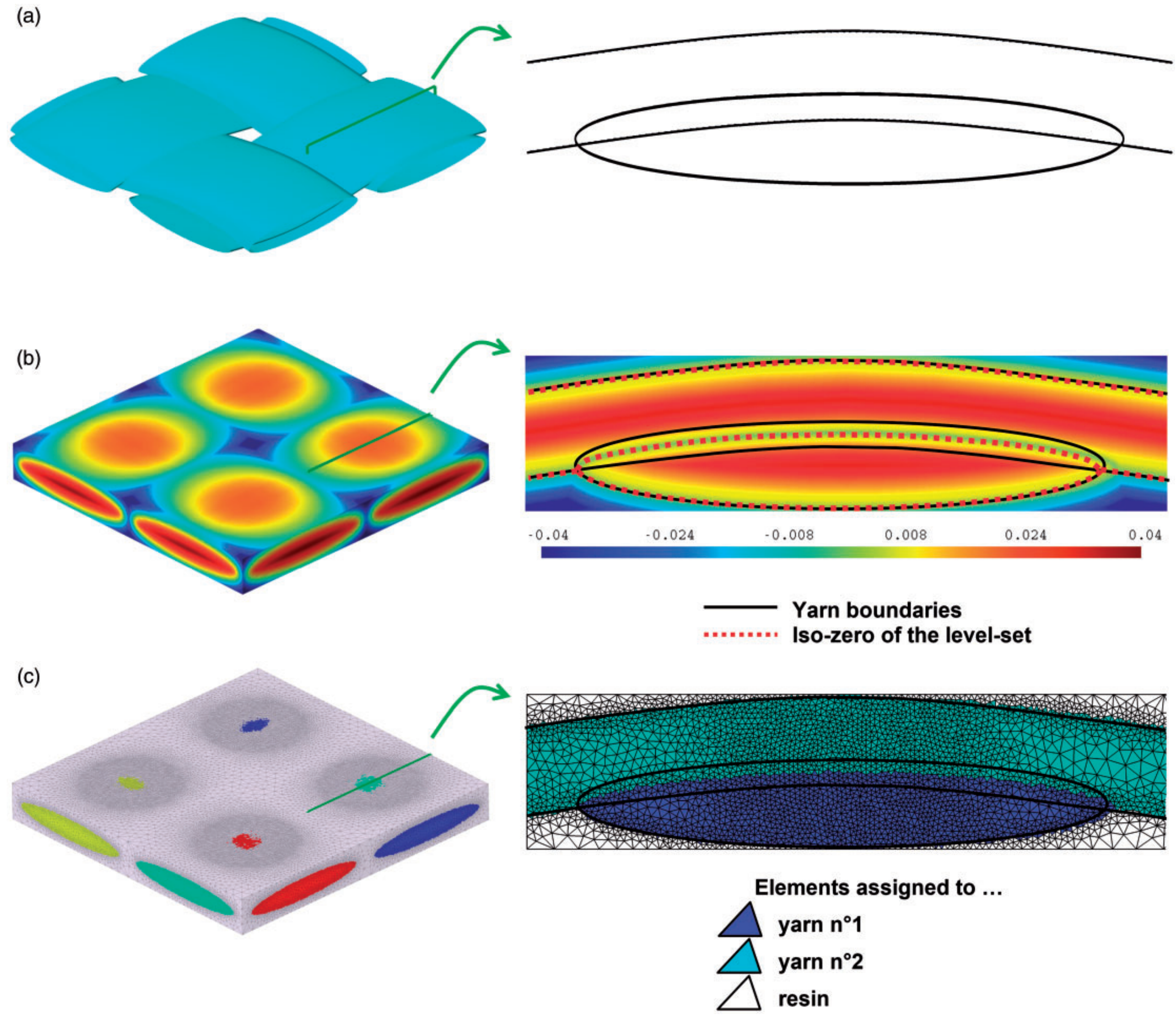

Figure 2. (a) Typical plain-weave textile modeled in TexGen without post-treatment. The cut view shows the penetrations due to the large volume fraction of yarns; (b) a level-set is computed, enabling to detect the yarn-resin and yarn-yarn interfaces, even in the penetration zones; (c) based on the level-set, a nonconformal mesh refined at the interfaces is built and each element is classified into the relevant entity.

mesh size gradient, usually between 0.8 and 1. The variable s is minimum at the iso-zero of the level-set d, highlighted for instance in Figure 2(b). This implies that the finest mesh sizes are enforced at the yarn–resin and yarn–yarn interfaces. The latter does not necessarily coincide with yarn boundaries, as evidenced by Figure 2(c). The FE mesh is periodic over the entire RVE so that opposite faces match, as imposed by the definition of the RVE. This is ensured by duplicating the textile geometry in all directions of periodicity, so that the distance field d becomes periodic. As illustrated in Figure 2(c), the signed distance field assigns each element to the relevant entity (resin, yarn no. 1, yarn no. 2, etc.) for the subsequent homogenization analysis, based on the position of its centroid. Each element is thus related to the appropriate material properties and orientation of the yarn to which it belongs to. The 3D mesh of Figure 2(c) has 344,000 nodes with first-order elements. It is compared with a voxel mesh in the cut view in Figure 3. This voxel mesh holds a similar amount of nodes as the unstructured mesh. The yarn boundaries appear much smoother in the case of the present meshing methodology than in the classical voxel approach. In that sense, the number of degrees of freedom is rationalized because the mesh is refined only where needed. The same is valid for second-order meshes, albeit to a lesser extent since second-order conversion multiplies the number of nodes by a larger factor in the case of tetrahedral elements compared to the case of voxels.

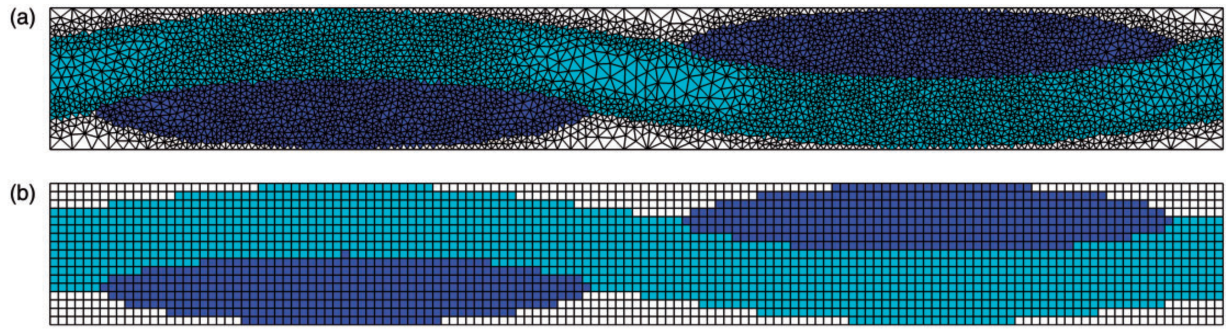

Figure 3. Comparison between (a) the meshing technique used in this work and (b) the voxel approach for the same number of nodes on a plain-weave textile. These meshes contain 344,000 and 363,000 nodes, respectively.

Homogenization of penetrating textiles

Principle of the compensation of penetrations

The objective of the methodology is to compute an accurate estimation of the homogenized thermomechanical properties in a complex textile with a minimum effort spent on textile modeling. Thus, simplified models of complex textiles are generated in the open-source, user-friendly textile modeler TexGen. The main characteristics of the textiles, i.e. fiber content, yarn crimp, and yarn volumes, are respected. The present method assumes simple sinusoidal or piecewise linear yarn mid-lines, depending on the textile architecture. Yarn cross-sections are constant with trivial shapes, either elliptical or rectangular. They are modeled to be as representative as possible of the complex reference model. If relevant, e.g. for 3D textiles, these cross-sections are further rotated about the mid-line of the yarns allowing for parallel major axes of the warp and weft cross-sections at contact points. In essence, this method induces penetrations between the yarns. In this section, a strategy is proposed to correct for the errors generated because of these penetrations.

The strategy is based on the following considerations:

- The volume of a yarn can be defined in three different ways, illustrated in Figure 4: by the nominal geometrical volume as defined in TexGen V_y, by the meshed volume of the yarn $V_{y,nc}$ as if the yarn was alone in the textile, and by the meshed volume accounting for penetrations $V_{y,p}$. The latter is the volume of the elements classified in the yarn, in the sense of Figure 2(c). Since a non-conformal approach is used, $V_{y,nc}$ is not necessarily equal to V_y. Moreover, $V_{y,p}$ can be smaller than $V_{y,nc}$, depending on the magnitude of the penetrations;
- Since the homogenized properties of the textile are mainly driven by the fiber content in all directions, it is of paramount importance to guarantee a realistic representation of the fiber content in each yarn. However, since the yarn volumes differ between the geometrical and nonconformal representations, the fiber content cannot be identical unless the intra-yarn fiber volume fraction is modified.

Since $V_{y,p}$ is the yarn volume entering the FE simulation, and V_y is the reference yarn volume, the idea is to preserve the fiber volume when transitioning from V_y to $V_{y,p}$, i.e. to find a corrected intra-yarn fiber volume fraction $k_{f,p}$ that fulfills

$$V_{y,p}k_{f,p} = V_y k_f \tag{3}$$

where k_f is the constant, reference intra-yarn fiber volume fraction in the geometrical representation. This is naturally achieved by using

$$k_{f,p} = \frac{V_y}{V_{y,p}} k_f \tag{4}$$

This adaptation is only based on global considerations and does not take local yarn intersections into account. An enhanced correction is proposed, accounting for local penetrations. To this end, the yarn mesh $V_{y,nc}$ is separated into an arbitrary number of cells (see Figure 5). In practice, each yarn is divided into 15–30 cells over the RVE length, depending on its geometrical complexity. While all elements lie within the yarn boundary, they are not all assigned to this particular yarn in the FE simulation. Hence, each cell i can be composed of two types of elements (see Figure 6).

The elements that are classified in the yarn contribute to the volume V_p^i, and the elements that are assigned to other yarns contribute to the volume V_o^i. In essence, the fiber volume that is supposed to be contained in V_o^i is lost in the FE simulation and must be added to V_p^i. This transition artificially mimics the compaction of all

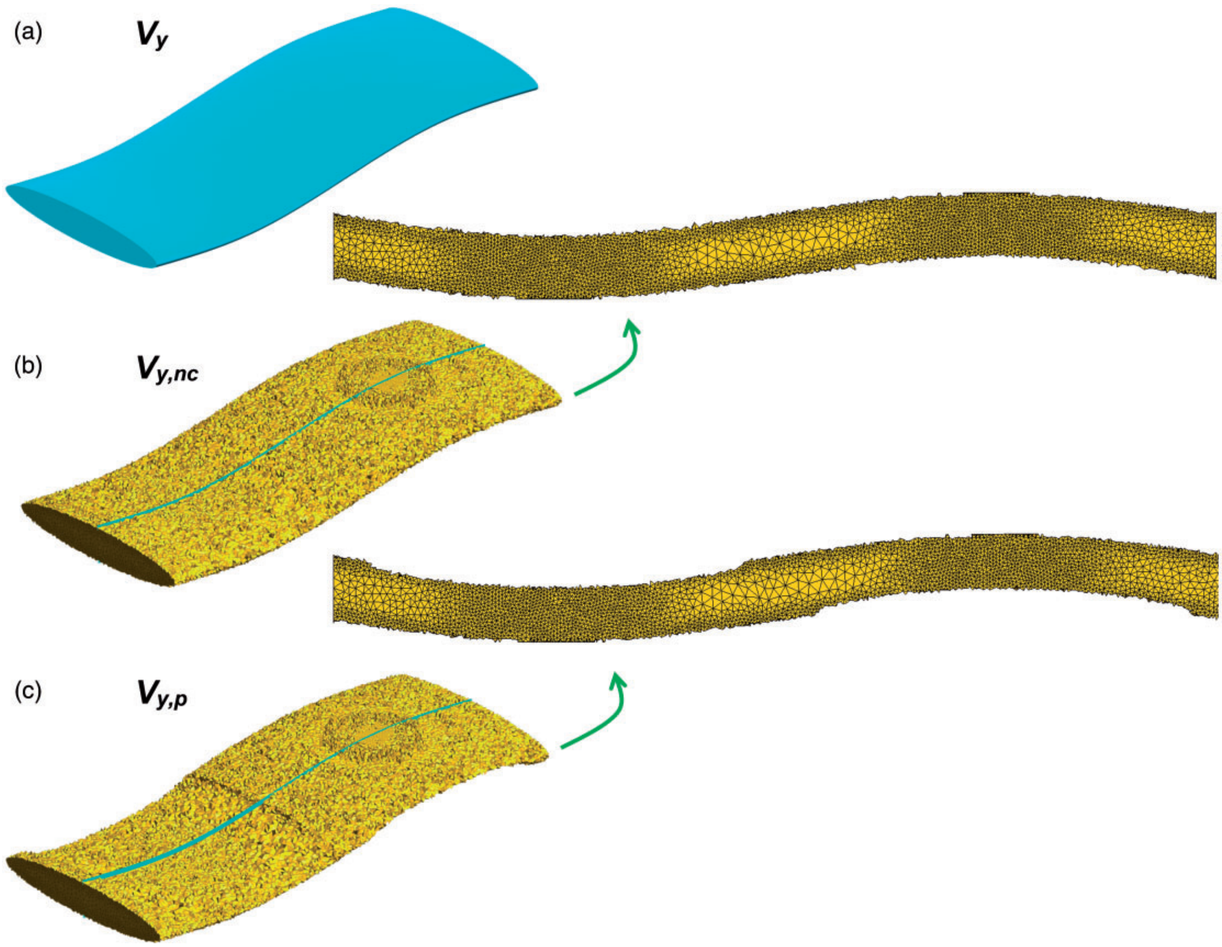

Figure 4. Definitions of (a) the geometrical volume V_y; (b) the meshed nonconformal volume of the yarn, as if the yarn was alone in the textile $V_{y,nc}$; (c) the volume of the elements $V_{y,p}$ that are assigned to the yarn.

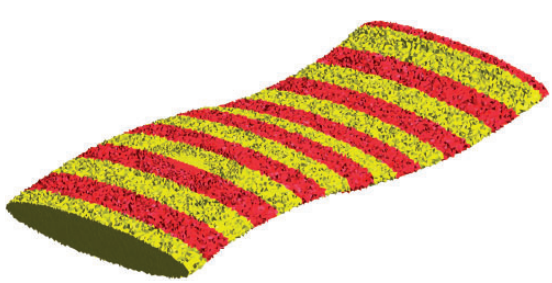

Figure 5. Division of a yarn into several cells for the procedure of local fiber volume fraction adaptation.

the fibers of cell i into the FE volume V_p^i. It is achieved by adapting the intra-yarn fiber volume fraction in the cell i as

$$k_{f,p}^i = \frac{V_y\left(V_p^i + V_o^i\right)}{V_{y,nc}V_p^i}k_f \tag{5}$$

Summation over i in equation (5) fulfills the requirement expressed by equation (3). Both equations (4) and (5) are valid also in the absence of penetrations or if more than two yarns overlap at the same location, and compensate for the mesh-related discretization error as well as the penetration-related fiber volume loss.

When the penetration volume is too large, equation (5) can lead to unrealistic values of intra-yarn fiber volume fraction $k_{f,p}^i$. Hence, a realistic upper limit is imposed to $k_{f,p}^i$ (e.g. 0.75, Green et al.[27]). If this limit is exceeded, an algorithm looks for the highest local fiber volume fraction, in the cell noted c, and for its two closest neighboring cells, in opposite directions along the yarn path, which do not exceed the limit. Then, half of the excess fiber volume in cell c is transferred to each of those two cells. The algorithm runs while there is at least one cell over the limit. It fails only if all cells exceed the limit, which means that the overall penetration within the yarn is too large. It can then be decided to increase the upper limit, or to improve the

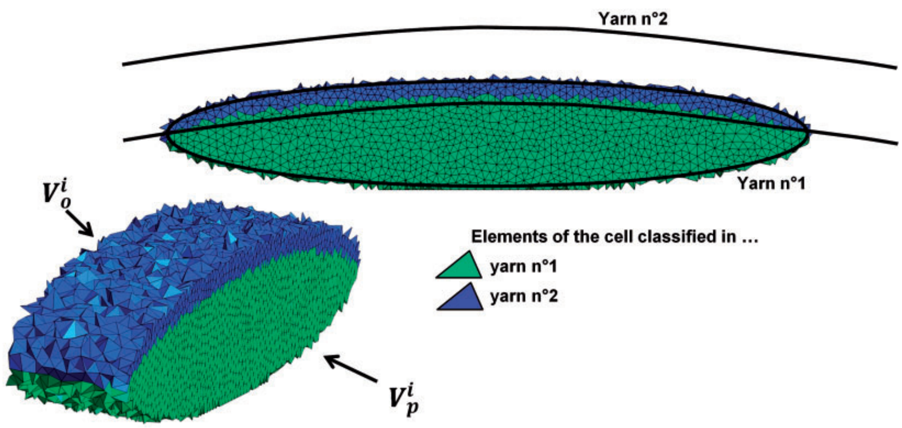

Figure 6. 3D and planar view of a yarn cell.

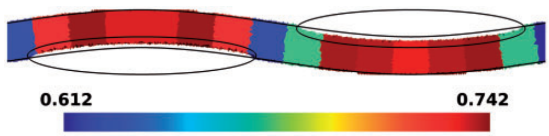

Figure 7. Distribution of the factor $k^i_{f,p}$ used to correct the fiber volume fraction along one yarn of the plain-weave textile. The black continuous line represents the yarn boundaries.

geometrical representation in order to reduce penetrations.

The resulting fiber volume fraction distribution $k^i_{f,p}$ over one yarn of the plain-weave discussed before is shown in Figure 7, with a nominal fiber volume fraction $k_f = 0.6$. The highest values of $k^i_{f,p}$ indeed appear where the yarn cross-sections are the most compacted due to penetrations with other yarns. None of the cells exceeds the upper limit, 0.75.

This method is generic and automated. It emulates changes in cross-section shapes and yarn compaction in the FE representation, while maintaining idealized and simple geometric modeling. After computing the local fiber volume fraction, using equation (5), the material properties must be determined in each cell of each yarn. Considering impregnated yarns as unidirectional composites allows the use of micromechanics-based models proposed by Chamis[35] to compute the yarn material properties. For the coefficient of thermal expansion (CTE) of the yarns, the models by Schapery[36] and Hyer[37] are used for the longitudinal and transverse directions, respectively. These models are presented in brief in the Appendix.

Finally, the homogenization of the complete RVE is tackled through the classical periodic FE procedure, where periodic boundary conditions are applied to compute the average stiffness tensor of the composite.[38–41]

Comparison to voxel meshing

A convergence study is performed to compare the accuracy of the present meshing technique, referred to as ‘‘unstructured’’ meshing, versus the classical voxel approach. The plain-weave similar to Figure 2 is considered except that penetrations are removed. Reference results are then generated with a conformal mesh. The convergence with conformal meshes is very fast and the results are thus considered as the exact reference solution. For both the unstructured and voxel meshes, the discretization error is compensated for owing to equation (4) and typical properties for carbon/epoxy are used for the constituents. Figure 8 presents the results of the convergence study. For each property, the relative error between the nonconformal mesh and the converged conformal results is calculated. The mean error, i.e. the averaged error over all properties, is 2.5 times less in the unstructured approach compared to voxels for the same number of nodes. At 200,000 nodes, no error is above 3.3% in the unstructured case, while three properties are still above 5% for voxels, with a particularly slow convergence for the in-plane CTE α_1. The unstructured mesh converges slower than voxels for the following properties:

- The out-of-plane shear modulus G_{13}, due to shear locking of the tetrahedral elements;
- The through-thickness Young's modulus E_3. This seems to be the consequence of the presence of a thin resin layer between the yarns. This artificial layer is added to be able to generate a conformal mesh. In the case of the voxel mesh, the layer is not captured, since the elements are not refined at the interface. While for the unstructured mesh, the irregular and thin nature of the layer is detrimental to the accurate prediction of the local stress field. However, the purpose of the layer is solely to compare to the conformal mesh.

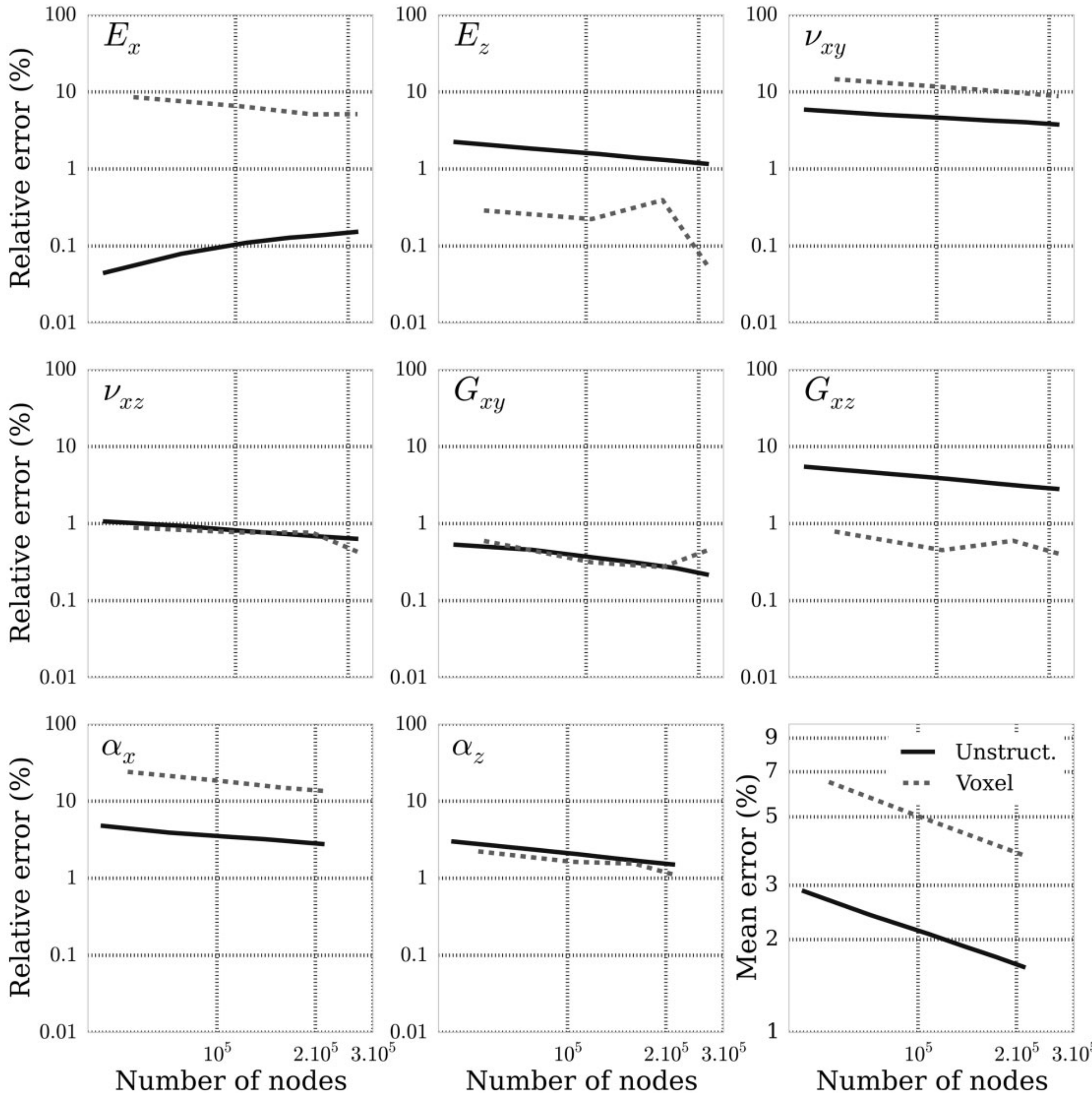

Figure 8. Accuracy of homogenization of a typical plain-weave with nonconformal meshes (unstructured and voxels) compared to reference results obtained with a conformal mesh. 1 and 2 are the in-plane directions, 3 is the through-thickness direction. *E*, ν, *G*, and α refer to Young's moduli, Poisson's ratios, shear moduli, and CTE, respectively.

However, on average, it is much more beneficial to use an unstructured mesh, which is refined locally at the material interfaces, instead of being uniform for the voxel counterpart.

Sensitivity analyses

A sensitivity study is conducted on the fictitious case in Figure 9. The reference configuration represents a penetration-free RVE that could have been produced by a complex textile modeling technique. The idealized configuration in Figure 9 represents the simplified textile in accordance with the present method. It respects the main characteristics of the reference configuration, such as the position of the mid-lines of the yarns, and the yarn volumes. The purpose of the sensitivity study is to assess the accuracy of the method, the influence of the yarn aspect ratios and the adequacy of equation (5) to compensate for the penetrations.

First, the sensitivity of the homogenization results with respect to the aspect ratio of the yarn cross-section is studied. This is important, since the geometrical

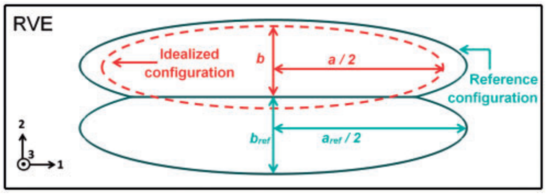

Figure 9. The reference configuration without penetration, vs the idealized configuration keeping yarn mid-lines and volumes. For clarity, only one yarn is illustrated in the idealized configuration.

simplification imposed in our method often leads to differences in the aspect ratio compared to more complex modeling approaches. The aspect ratio r of the idealized configuration is defined by the ratio between the minor axis and the major axis of the yarn after meshing and element classification, illustrated in Figure 9 as $r = b/a$. The term r_{ref} refers to the aspect ratio in the reference configuration, computed as b_{ref}/a_{ref}. Figure 9 depicts the situation $r = r_{ref} = 0.2$. Even when $r = r_{ref}$, the reference and idealized configurations are not equal because the areas of the ellipses in the idealized textile are equal to the cross-section areas of the reference yarns, which are not ellipses. The sensitivity study consists in performing homogenization analyses when r varies within $r_{ref} \pm 10\%$, and comparing to the reference results without any penetrations.

Then, it is checked that equation (5) is the best way to compensate textile penetrations. This is evaluated by multiplying the result of equation (5) by a factor of 1 ± 0.1, which is equivalent to changing k_f by $\pm 10\%$ with respect to the reference value $k_{f,ref}$. In this case, $k_{f,ref} = 0.7$ is chosen. Since the yarns are here straight, global and local corrections by equations (4) and (5), respectively, give equivalent results.

The results are presented in Figures 10 and 11 for the sensitivity with respect to the aspect ratio of the cross-section and to the correction for the fiber content equation (5), respectively. In each figure, one graph for each of the 12 orthotropic properties shows the value obtained by the idealized model normalized by the value of the reference configuration. Moreover, the mean error over all predicted properties (with identical weights for each property) is computed. Figure 10 also shows the results obtained when the aspect ratio varies and the penetrations are not corrected, i.e. $k_{f,p} = k_{f,ref}$. The main findings are the following:

- Trends are conflicting, meaning that increasing or decreasing r or k_f leads to better accuracy for some properties and to reduced accuracy for others.
- When averaging the accuracy over all properties, the mean error reaches a minimum of 0.4% for $r = r_{ref}$ and $k_f = k_{f,ref}$, which means that using the same aspect ratio and fiber content as in the reference configuration is indeed the best possible choice. The associated maximum error is observed for G_{23} and is about 2%. Changing the aspect ratio or the fiber content slightly does not help improving the compensation for the penetrations.
- The same configuration without correcting for the penetrations leads to a mean error of 5%, i.e. 10 times larger than when the correction is used. The maximum error reaches 13% for the longitudinal CTE α_3.
- The mean error stays below 1.5% in the range $r_{ref} \pm 10\%$, and below 6% in the range $k_{f,ref} \pm 10\%$. This means that, for the present test case and for the evaluated elastic properties, the accuracy of the homogenization procedure is more sensitive to variations in the fiber content than in the aspect ratio. This implies, as expected, that it is of primary importance to use a corrected fiber volume fraction in the simplified approach, with the help of equation (5). The yarn aspect ratio, on the other hand, has a subordinate effect on the accuracy.
- The shear moduli G_{23} and G_{13}, the transverse CTE α_2 and the Poisson's ratio υ_{12} are the most sensitive to the yarn aspect ratio, with errors up to 5%, 4.5%, 3%, and 2.5%, respectively, when $r = r_{ref} \pm 10\%$.

In the aspect ratio sensitivity study, the penetration volume varied from 3% to 5% of the total volume of the RVE, increasing with r.

Comparison to cases from the literature

In this section, the new nonconformal methodology is compared to results published in the literature for 3D textiles. For details about the modeling approaches used by the respective authors, the reader is referred to the referenced papers. Details necessary to reproduce the results obtained by our approach, such as the geometrical information or material properties, can be found in Table 1. The comparison between the new approach and the reference results is summarized for all test cases in Table 2.

Case 1

A typical application of the proposed methodology is the modeling of complex, highly compacted 3D textiles. Stig and Hallström[9,29] developed a modeling framework suited to such textiles. Yarns are modeled as shells and are inflated with contact conditions by running a first explicit FE analysis until a desired yarn volume fraction is reached. For the cases addressed here, the geometrical fidelity with respect to the manufactured textile is remarkable. The yarns occupy up to 85% of the volume of the RVE.[9] Such compaction

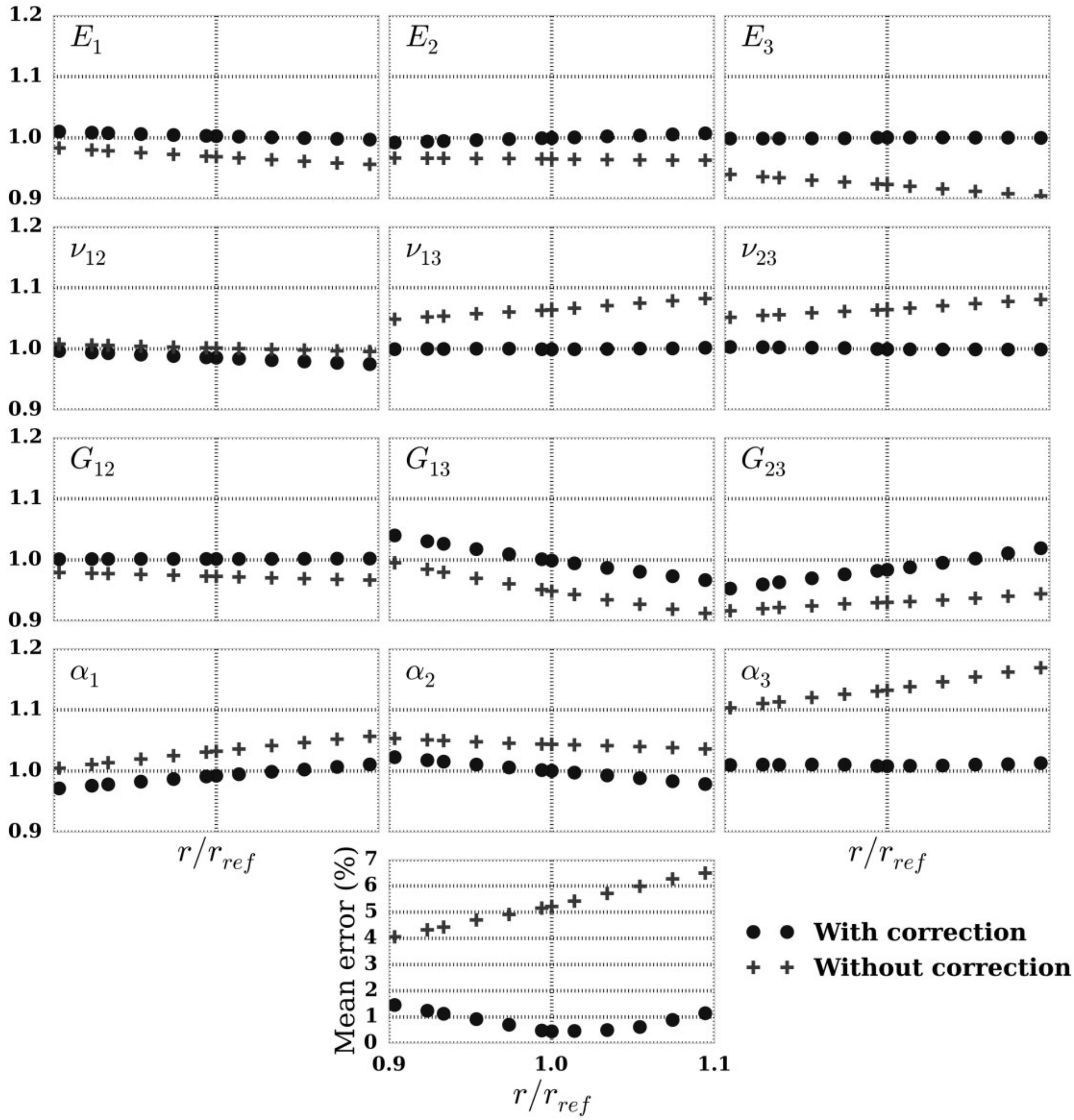

Figure 10. Influence of the aspect ratio r normalized by the reference value r_{ref} on the accuracy of the predictions of the different elastic constants and on the mean error on all these predictions.

without yarn penetrations is out of reach with built-in functionalities of TexGen since the yarn cross-section varies significantly both in size and shape along its length. The simplified modeling strategy suggested here was applied to some of the test cases presented in Stig and Hallström[9] using the following parameters:

- Identical dimensions of the RVE as in the reference case.
- Similar yarn paths and yarn interlacing, from a topological point of view, as in the reference case. The yarn topology is illustrated in Figure 12(a), defined by simple sinusoidal functions, with amplitudes set to represent, on average, the prescribed crimp of the reference case.
- Constant and elliptical yarn cross-sections. The area of the cross-sections are given by the fiber count (12 k for warp yarns, 6 k for weft yarns) and by the assumption that the average intra-yarn fiber volume fraction is the same for all yarns.[9] The amplitudes of the yarn paths are calculated so that warp and weft yarns are tangent at contact points. A simple

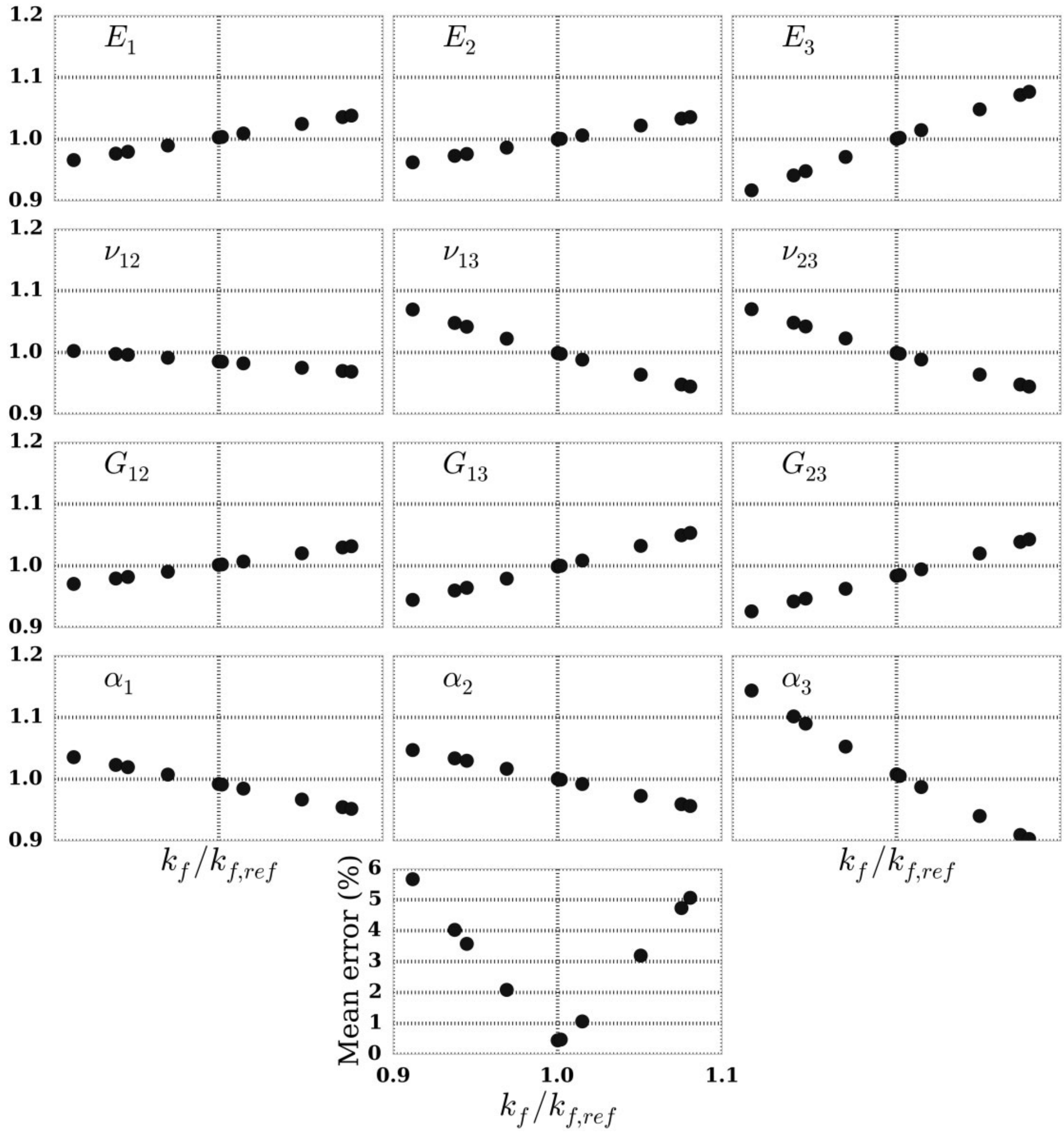

Figure 11. Influence of the fiber volume fraction k_f normalized by the reference value $k_{f,ref}$ on the accuracy of the predictions of the different elastic constants and on the mean error on all these predictions.

algorithm, implemented in the user interface of TexGen, selects the aspect ratio of the ellipses in order to minimize the overall amount of penetration in the RVE. The cross-section of warp yarns is progressively rotated along the yarn path so that the major axes of the yarns are parallel at the contact points.

No further hypothesis is needed to model the textile. It takes TexGen about 5 min on a typical desktop computer to find the configuration that minimizes yarn penetrations. Three textiles are reproduced from Stig and Hallström,[9] referred to as S, B, and D, in agreement with the notation used in the previous work. They have the same textile architecture, but different RVE dimensions, fiber contents, yarn crimp, etc. For illustration, the simplified model of textile B is shown in Figure 12(b). The penetration volume, i.e. the volume that is occupied by more than one yarn, is 9.7% of the total volume of the RVE. All

Table 1. Summary of all the geometrical and material parameters used for the test cases in "Comparison to cases from the literature" section. The subscripts L and T stand for longitudinal and transverse directions, respectively.

	Case 1, Textile S	Case 1, Textile B	Case 1, Textile D	Case 2	Case 3
RVE dimensions $X \times Y \times Z$ (mm^3)	$17.72 \times 2.12 \times 2.12$	$11.74 \times 2.18 \times 2.18$	$7.47 \times 2.33 \times 2.33$	$6.64 \times 5.03 \times 2.7632$	$5.44 \times 1.57 \times 2.79$
Warp yarns cross-section (mm^2)	Elliptical 1.57×0.71	Elliptical 1.63×0.66	Elliptical 1.68×0.58	Rectangular 4.12×0.637	Rectangular 0.90×0.19
Weft yarns cross-section (mm^2)	Elliptical 2.94×0.19	Elliptical 2.73×0.20	Elliptical 2.01×0.24	Rectangular 0.292×1.514	Rectangular 0.96×0.22
Vertical yarns cross-section (mm^2)	Elliptical 2.94×0.19	Elliptical 2.73×0.20	Elliptical 2.01×0.24	Rectangular 0.910×0.292	Elliptical 0.67×0.32
Yarn mid-line (warp yarns)	Helicoidal, amplitude 0.44 mm	Helicoidal, amplitude 0.42 mm	Helicoidal, amplitude 0.40 mm	Piecewise linear	Piecewise linear
Yarn mid-line (weft/vertical yarns)	Sinusoidal, amplitude 0.0095 mm	Sinusoidal, amplitude 0.0098 mm	Sinusoidal, amplitude 0.0105 mm	Piecewise linear	Piecewise linear
Intra-yarn fiber volume fraction k_f (%)	54	54	57	70.2	Warp: 92.0[a] Weft: 70.2 Vertical: 51.0
Total fiber volume fraction (%)	45	44	42	49	43
Penetration volume fraction (%)	10.5	9.7	7.7	0.03	0.001
Matrix properties (isotropic)		Reichhold Dion 9500. $E = 3.1$ GPa, $\upsilon = 0.35$		Dow Derakane 8084. $E = 3.53$ GPa, $\upsilon = 0.35$	Epicote 828. $E = 2.2$ GPa, $\upsilon = 0.35$
Fiber properties		T700 carbon fibers. Orthotropic: $E_L = 230$ GPa, $E_T = 14$ GPa, $\upsilon_{LT} = 0.2$, $\upsilon_{TT} = 0.25$, $G_{LT} = 9$ GPa, $G_{TT} = 4.8$ GPa		S-2 glass fibers. Isotropic: $E = 86.9$ GPa, $\upsilon = 0.22$	T300 carbon fibers. Transverse isotropic: $E_L = 220$ GPa, $E_T = 13.8$ GPa, $\upsilon_{LT} = 0.2$, $\upsilon_{TT} = 0.25$, $G_{LT} = 11.35$ GPa
Yarn properties		Micromechanics		From Bogdanovich[42]	Micromechanics

[a]Such a high value is unrealistic but necessary to achieve the declared overall fiber content in the warp direction, based on the geometrical description of the RVE given by the authors.

homogenization results are presented in Table 1. The columns "global correction" and "local correction" refer to the results obtained using equations (3) and (4), respectively.

The comparison between the results obtained with the local correction and the reference finite element predictions demonstrates an average difference of 10% for the elastic modulus (6% if the worst of the six predictions is discarded) and for the shear modulus. However, the Poisson's ratios are systematically underestimated, by 15–35%. This deviation is, however, not surprising since the predicted transverse contraction is likely to be more sensitive to the geometrical assumptions that were made, in particular the constant yarn cross-sections. The present methodology complies very well with the experimental data presented in Stig and Hallström[9] for the modulus in the warp direction, in fact equally well or better than the reference FE results. However, as stated in Stig and Hallström,[9,29] the models are perfectly regular and periodic while the material in the experiments was not, due to semi-manual manufacturing, and the experimental data was based on only a few

Table 2. Comparison of homogenization results for all test cases. The presented relative difference is between the local correction and the experimental results, and all moduli are expressed in GPa.

	Present, local correction	Present, global correction	Reference, numerical	Reference, experimental	Relative difference (%)
Case 1, Textile S[9]					
E_x	74.7	77.1	83.2	74.6 ± 0.3	+0.1
E_y	11.7	11.7	12.0		
υ_{xy}	0.26	0.26	0.31		
υ_{yz}	0.27	0.25	0.31		
G_{xy}	3.26	3.29	3.76		
G_{yz}	1.93	2.27	1.93		
Case 1, Textile B[9]					
E_x	59.0	60.7	65.8	58.8 ± 3.7	+0.3
E_y	13.3	13.2	12.5		
υ_{xy}	0.27	0.27	0.36		
υ_{yz}	0.23	0.22	0.28		
G_{xy}	3.35	3.35	3.94		
G_{yz}	1.94	2.25	1.99		
Case 1, Textile D[9]					
E_x	36.2	36.4	36.2	31.9 ± 2.1	+13.5
E_y	15.0	14.9	11.5		
υ_{xy}	0.26	0.26	0.41		
υ_{yz}	0.18	0.17	0.27		
G_{xy}	3.08	3.12	3.84		
G_{yz}	1.95	2.23	2.19		
Case 2[42]					
E_x	24.95		27.31	24.68	+1.1
E_y	20.44		25.70	20.75	−1.5
υ_{xy}	0.119		0.125	0.11	+8.2
G_{xy}	3.15		3.58	3.86	−18.4
Case 3[43,44]					
E_x	41.88		39.70	40.97 ± 2.00	+2.2
E_y	48.64		51.09	47.30 ± 4.02	+2.8
υ_{xy}	0.031		0.033	0.0346 ± 0.01	−10.4

samples. As far as the Poisson's ratios are concerned, experimental data would be needed to make further conclusions.

The difference between the results obtained with the local and the global corrections is very small. The shear modulus G_{yz} is affected most, with the local correction providing the lower discrepancy with respect to the reference results for two out of three cases. Therefore, it cannot be stated from these test cases that the local correction yields better homogenization predictions, although its physical interpretation seems to be more realistic. Intuitive and simpler to implement, the global correction delivers satisfactory predictions, but it probably cancels out part of the stress and strain fields heterogeneity associated with local compaction. Of apparently limited importance for the computation of

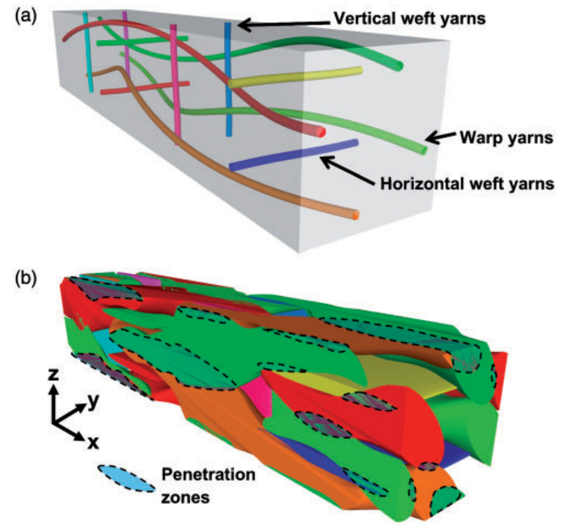

Figure 12. Case 1 (a) yarn paths of the 3D-woven textile; (b) 3D-woven textile B modeled in TexGen. Penetrations occupy 9.7% of the RVE volume.

homogenized properties, this difference might become relevant when addressing failure criteria within the yarns. However, more in-depth investigations are needed to demonstrate the benefits of the local approach. From a computational efficiency perspective, the local correction induces a negligible pre-treatment computational cost: in the presented case, less than 2 min per million elements.

Cases 2 and 3

Two other 3D textiles were developed and tested by Bogdanovich[42] and Tan et al.[43,44] These textiles are replicated in TexGen using built-in functionalities only, and shown in Figure 13. The reference models are already simplified versions of the real textile, which implies that:

- The models generated in TexGen in the present work are very similar to the reference geometries. On the one hand, the textile of Bogdanovich,[42] which was composed of straight rectangular in-plane yarns and inclined vertical yarns, is further simplified for the present methodology following the representation by Rao et al.[45] On the other hand, the textile in Tan et al.[44] was modeled with straight yarns using rectangular cross-sections.
- The penetrations are solely located at the corner of the vertical yarns, occupying less than 0.05% of the total volume, which is thus negligible. In such cases, equation (5) gives $k^i_{f,p} \approx k_f$, since $V^i_0 \ll V^i_p$. Therefore, the correction procedure has no impact and the homogenization behaves classically.

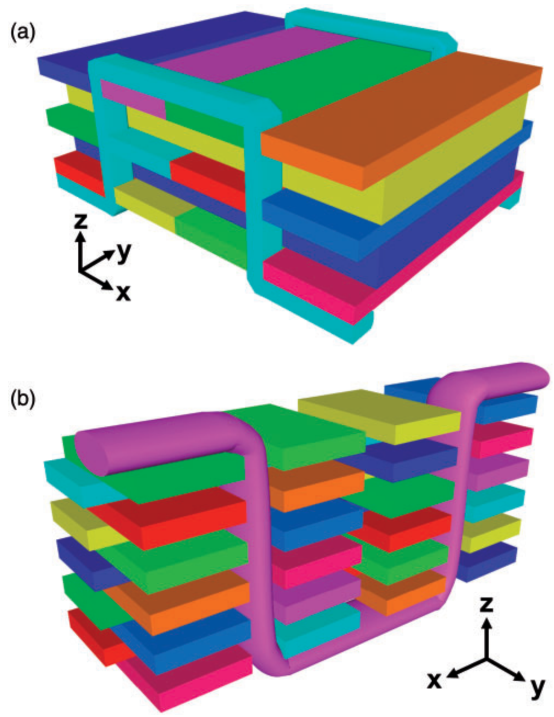

Figure 13. TexGen models of the 3D-woven textiles (a) case 2; (b) case 3.

Therefore, these two cases do not validate the penetration correction method, but only the simplified geometrical representation combined with the nonconformal meshing approach. Results from the comparison are presented in Table 1. The overall correlation is quite satisfactory. In particular, the relative error of the presented methodology compared to experimental results is 1% to 3% for Young's moduli. It is 10% or less for Poisson's ratios, for which the experimental variability is likely to be high, and 18% for the in-plane shear modulus in case 2.

Conclusion

A nonconformal meshing is proposed allowing FE homogenization of penetrating textile geometries without FE or geometrical pre-treatment, aside from a specific but fast mesh adaptation step. The methodology is not limited by the amount or location of the penetrations and proved to be successful up to penetrations of 10% in volume. However, the physical fidelity of the model diminishes in cases of exaggerated penetration volumes. The main benefits of the method are:

- Very limited effort is required to generate geometrical representations of a very wide range of textiles, after which no user intervention is necessary throughout the entire homogenization process.
- Small or large yarn overlaps are not obstacles to the FE simulations, discarding the need for complex pre-treatment to remove penetrations that are bound to appear when modeling highly compacted architectures.
- Even with a penetration-free textile, the methodology has the advantage of leaving full control to the user over the mesh size and, hence, over the computational time, as opposed to conformal meshes that may require very fine elements in thin resin regions and large computational times. With the non-conformal approach, fine elements at yarn interfaces lead to improved predictions, but this is not mandatory.

The computational chain is composed of several steps: textile modeling, distance field computation, meshing, FE analysis, and post-treatment. Of those steps, only the distance field computation and the FE analysis last for more than a few minutes. The distance field computation takes about 1 h per million nodes on a typical desktop computer and it can be parallelized for further speed-up. Most of the computational time lies in the FE analysis and depends on the mesh size, the software and the parallelization capabilities, as for every FE-based homogenization procedure. Mesh sensitivity was not at the core of the present work. Therefore, it was not studied for all test cases. For textile B (case 1), convergence was achieved with 700,000 nodes which is reasonable.

Future investigations will include the evaluation of the accuracy of this methodology in the context of non-linear material behavior, for instance progressive failure. Particular care should be taken because of the local stress concentrations related to the non-conformal approach. The mesh refinement procedure that was developed is expected to help in that respect compared to the voxel approach, in light of the faster convergence which has been evidenced. However, it may be anticipated that the level of geometrical fidelity will need to be improved, and that finer models, e.g. of fiber re-alignment in penetration zones, must be enforced. Another possible improvement is the use of anisotropic mesh refinement, as done e.g. by Quan et al.,[46] where yarn curvature is taken into account to drive the mesh size and further optimize the number of nodes. Finally, the approach should be further tested and validated against other modeling techniques, with more experimental data.

Declaration of Conflicting Interests

The author(s) declared no potential conflicts of interest with respect to the research, authorship, and/or publication of this article.

Funding

The author(s) disclosed receipt of the following financial support for the research, authorship, and/or publication of this article: This work was supported by the Walloon Region (Belgium) through the First DoCA project OPTIMOLD (grant number ECV320600FD012F / 1117310).

References

1. Ishikawa T and Chou TW. Stiffness and strength behaviour of woven fabric composites. *J Mater Sci* 1982; 17: 3211–3220.
2. Vandeurzen P, Ivens J and Verpoest I. A three-dimensional micromechanical analysis of woven-fabric composites. I. Geometric analysis. *Compos Sci Technol* 1996; 56: 1303–1315.
3. Vandeurzen P, Ivens J and Verpoest I. A three-dimensional micromechanical analysis of woven-fabric composites. II. Elastic analysis. *Compos Sci Technol* 1996; 56: 1317–1327.
4. Paley M and Aboudi J. Micromechanical analysis of composites by the generalized cells model. *Mech Mater* 1992; 14: 127–139.
5. Prodromou AG, Lomov SV and Verpoest I. The method of cells and the mechanical properties of textile composites. *Compos Struct* 2011; 93: 1290–1299.
6. Gommers B, Verpoest I and van Houtte P. The Mori-Tanaka method applied to textile composite materials. *Acta Mater* 1998; 46: 2223–2235.
7. Huysmans G, Verpoest I and van Houtte P. A poly-inclusion approach for the elastic modelling of knitted fabric composites. *Acta mater* 1998; 46: 3003–3013.
8. Lomov SV, Ivanov DS, Verpoest I, et al. Meso-FE modelling of textile composites: Road map, data flow and algorithms. *Compos Sci Technol* 2007; 67: 1870–1891.
9. Stig F and Hallström S. A modelling framework for composites containing 3D reinforcement. *Compos Struct* 2012; 94: 2895–2901.
10. Ernst G, Vogler M, Hühne C, et al. Multiscale progressive failure analysis of textile composites. *Compos Sci Technol* 2010; 70: 61–72.
11. Straumit I, Lomov SV and Wevers M. Quantification of the internal structure and automatic generation of voxel models of textile composites from X-ray computed tomography data. *Compos Part A: Appl Sci Manuf* 2015; 69: 150–158.
12. Green SD, Matveev MY, Long AC, et al. Mechanical modelling of 3D woven composites considering realistic unit cell geometry. *Compos Struct* 2014; 118: 284–293.
13. Zeng X, Brown LP, Endruweit A, et al. Geometrical modelling of 3D woven reinforcements for polymer composites: Prediction of fabric permeability and composite mechanical properties. *Compos Part A: Appl Sci Manuf* 2014; 56: 150–160.
14. Hello G, Schneider J and Aboura Z. Numerical simulations of woven composite materials with voxel-FE models. In: *Proceedings of ECCM-16 conference*, Seville, Spain, 22–26 June 2014.
15. Potter E, Pinho ST, Robinson P, et al. Mesh generation and geometrical modelling of 3D woven composites with variable tow cross-sections. *Comp Mater Sci* 2012; 51: 103–111.
16. Kim HJ and Swan CC. Voxel-based meshing and unit-cell analysis of textile composites. *Int J Numer Meth Eng* 2003; 56: 977–1006.
17. Crookston JJ, Ooi JW, Zhao LG, et al. Finite element analysis of textile composite unit cells using conventional and novel techniques. In: *Proceedings of ICCM-15 conference*, Durban, South Africa, 27 June to 2 July 2005.
18. Iarve EV, Mollenhauer DH, Zhou EG, et al. Independent mesh method-based prediction of local and volume average fields in textile composites. *Compos Part A: Appl Sci Manuf* 2009; 40: 1880–1890.
19. Nakai H, Kurashiki T and Zako M. Individual modeling of composite materials with mesh superposition method under periodic boundary condition. In: *Proceedings of ICCM-16 conference*, Kyoto, Japan, 3–8 July 2007.
20. Cox BN, Carter WC and Fleck NA. A binary model of textile composites — I. Formulation. *Acta Metall Mater* 1994; 42: 3463–3479.
21. Lomov SV, Verpoest I, Cichosz J, et al. Meso-level textile composites simulations: Open data exchange and scripting. *J Compos Mater* 2014; 48: 621–637.
22. Verpoest I and Lomov SV. Virtual textile composites software WiseTex: Integration with micro-mechanical, permeability and structural analysis. *Compos Sci Technol* 2005; 65: 2563–2574.
23. Lomov SV, Gusakov AV, Huysmans G, et al. Textile geometry preprocessor for meso-mechanical models of woven composites. *Compos Sci Technol* 2000; 60: 2083–2095.
24. Adam L and Assaker R. Integrated nonlinear multi-scale material modelling of fiber reinforced plastics with Digimat: Application to short and continuous fiber composites. In: *Proceedings of WCCM XI conference*, Barcelona, Spain, 20–25 July 2014.
25. Melchior MA, Duflot M, Gerard JS, et al. End-to-end FE based homogenization of woven composites. In: *Proceedings of ACCE conference*, Novi, USA, 9–11 September 2014.
26. Lin H, Brown LP and Long AC. Modelling and simulating textile structures using TexGen. *Adv Mater Res* 2011; 331: 44–47.
27. Green SD, Long AC, El Said BSF, et al. Numerical modelling of 3D woven preform deformations. *Compos Struct* 2014; 108: 747–756.
28. Mahadik Y and Hallett SR. Finite element modelling of tow geometry in 3D woven fabrics. *Compos Part A: Appl Sci Manuf* 2010; 41: 1192–1200.
29. Stig F and Hallström S. Spatial modelling of 3D-woven textiles. *Compos Struct* 2012; 94: 1495–1502.
30. Sonon B and Massart TJ. A level-set based representative volume element generator and XFEM simulations for textile and 3D-reinforced composites. *Materials* 2013; 6: 5568–5592.
31. Miao Y, Zhou E, Wang Y, et al. Mechanics of textile composites: Micro-geometry. *Compos Sci Technol* 2008; 68: 1671–1678.

32. Rinaldi RG, Blacklock M, Bale H, et al. Generating virtual textile composite specimens using statistical data from micro-computed tomography: 3D tow representations. *J Mech Phys Solids* 2012; 60: 1561–1581.
33. Grail G, Hirsekorn M, Wendling A, et al. Consistent Finite Element mesh generation for meso-scale modeling of textile composites with preformed and compacted reinforcements. *Compos Part A: Appl Sci Manuf* 2013; 55: 143–151.
34. Geuzaine C and Remacle JF. Gmsh: A three-dimensional finite element mesh generator with built-in pre- and post-processing facilities. *Int J Numer Meth Eng* 2009; 79: 1309–1331.
35. Chamis CC. Simplified composite micromechanics equations for strength, fracture toughness and environmental effects. *SAMPE Quart*1984.
36. Schapery RA. Thermal expansion coefficients of composite materials based on energy principles. *J Compos Mater* 1968; 2: 380–404.
37. Hyer MW. *Stress analysis of fiber-reinforced materials*, 2nd ed. Lancaster, PA: Destech Publications, Inc., 2009.
38. Labanieh AR, Legrand X, Koncar V, et al. Evaluation of the elastic behavior of multiaxis 3D-woven preforms by numerical approach. *J Compos Mater* 2014; 48: 3243–3252.
39. Wang XF, Wang XW, Zhou GM, et al. Multi-scale analyses of 3D woven composite based on periodicity boundary conditions. *J Compos Mater* 2007; 41: 1773–1788.
40. Xia Z, Zhang Y and Ellyin F. A unified periodical boundary conditions for representative volume elements of composites and applications. *Int J Solids Struct* 2003; 40: 1907–1921.
41. Li S and Wongsto A. Unit cells for micromechanical analyses of particle-reinforced composites. *Mech Mater* 2004; 36: 543–572.
42. Bogdanovich AE. Multi-scale modeling, stress and failure analyses of 3-D woven composites. *J Mater Sci* 2006; 41: 6547–6590.
43. Tan P, Tong L, Steven GP, et al. Behavior of 3D orthogonal woven CFRP composites. Part I. Experimental investigation. *Compos Part A: Appl Sci Manuf* 2000; 31: 259–271.
44. Tan P, Tong L, Steven GP, et al. Behavior of 3D orthogonal woven CFRP composites. Part II. FEA and analytical modeling approaches. *Compos Part A: Appl Sci Manuf* 2000; 31: 273–281.
45. Rao MP, Sankar BV and Subhash G. Effect of Z-yarns on the stiffness and strength of three-dimensional woven composites. *Compos Part B: Eng* 2009; 40: 540–551.
46. Quan DL, Toulorge T, Marchandise E, et al. Anisotropic mesh adaptation with optimal convergence for finite elements using embedded geometries. *Comput Method Appl M* 2014; 268: 65–81.

Appendix

Micromechanics-based models

The micromechanics-based models used to determine the properties of a unidirectional composite, as a function of the intra-yarn fiber volume fraction k_f, are given below. Equations (6) to (11) were developed by Chamis[35] for the elastic response, equation (12) was suggested by Schapery[36] for the longitudinal CTE, and equation (13) was suggested by Hyer[37] for the transverse CTE. The subscripts L and T stand for the longitudinal and transverse directions of the yarn, respectively. The subscripts y, f and r refer to yarn, fiber and resin properties, respectively.

$$E_{L,y} = k_f E_{L,f} + \left(1 - k_f\right) E_r \tag{6}$$

$$E_{T,y} = \frac{E_r}{1 - \sqrt{k_f}(1 - E_r/E_{T,f})} \tag{7}$$

$$G_{LT,y} = \frac{G_r}{1 - \sqrt{k_f}(1 - G_r/G_{LT,f})} \tag{8}$$

$$G_{TT,y} = \frac{G_r}{1 - k_f(1 - G_r/G_{TT,f})} \tag{9}$$

$$\upsilon_{LT,y} = k_f \upsilon_{LT,f} + \left(1 - k_f\right)\upsilon_r \tag{10}$$

$$\upsilon_{TT,y} = k_f \upsilon_{TT,f} + \left(1 - k_f\right)\left(2\upsilon_r - \frac{E_{T,y}}{E_{L,y}}\upsilon_{LT,y}\right) \tag{11}$$

$$\alpha_{L,y} = \frac{\alpha_{L,f} k_f E_{L,f} + \alpha_r\left(1 - k_f\right)E_r}{E_{L,y}} \tag{12}$$

$$\alpha_{T,y} = \alpha_r + \left(\alpha_{T,f} - \alpha_r\right)k_f + \frac{\upsilon_r E_{L,f} - \upsilon_{LT,f} E_r}{E_{L,y}}\left(\alpha_r - \alpha_{L,f}\right)(1 - k_f)k_f \tag{13}$$